Hindawi Publishing Corporation
Journal of Nanomaterials
Volume 2014, Article ID 964548, 7 pages
http://dx.doi.org/10.1155/2014/964548

Research Article

Role of Vanadium Pentoxide Hole-Extracting Nanolayer in Rubrene/C_{70}-Based Small Molecule Organic Solar Cells

Zhen Zhan,[1,2] Jing Cao,[1,2] Weiguang Xie,[1,2] Lintao Hou,[1,2,3] Qin Ye,[1,2] and Pengyi Liu[1,2,3]

[1] *Department of Physics, Jinan University, Guangzhou 510632, China*
[2] *Siyuan Lab, Jinan University, Guangzhou 510632, China*
[3] *State Key Laboratory of Luminescent Materials and Devices, South China University of Technology, Guangzhou 510632, China*

Correspondence should be addressed to Pengyi Liu; tlpy@jnu.edu.cn

Received 2 November 2013; Accepted 13 January 2014; Published 27 February 2014

Academic Editor: Yu-Lun Chueh

Copyright © 2014 Zhen Zhan et al. This is an open access article distributed under the Creative Commons Attribution License, which permits unrestricted use, distribution, and reproduction in any medium, provided the original work is properly cited.

Vanadium pentoxide (V_2O_5) was inserted between the donor layer and the anode as a hole-extracting nanolayer. Compared with devices without a hole-extracting layer, short-circuit current density (J_{SC}), open-circuit voltage (V_{OC}), fill factor (FF), and power conversion efficiency (PCE) of rubrene/C_{70}-based heterojunction solar cells with 3 nm V_2O_5 nanolayer are enhanced by 99%, 73%, 20%, and 310%, respectively. We found that V_2O_5 interlayer can effectively suppress the contact resistance and increase the hole transport capability. The dependence of the device performance on V_2O_5 layer thickness as well as fill factor on exciton dissociation and charge transport was also investigated in detail.

1. Introduction

Solar cells are presently considered as an important source of renewable and green energy to solve the energy crisis. Due to potential applications of compatibility with flexible substrates, low-manufacturing cost, and large-area fabrication [1–3], organic solar cells (OSCs) have received much attention as one kind of the most promising devices in energy harvesting area. Since the first discovery of donor-acceptor heterojunction cell by Tang [4], the performance of OSCs has greatly improved by the use of new materials [5], nanostructuring [6], and the modification of interfaces [7, 8].

Improvements in the performance of OSCs are commonly achieved by inserting a hole-extracting layer between the indium tin oxide (ITO) transparent conducting electrode and the organic donor materials. The hole-extracting layer improves the efficiency of hole transport from the active layer into the ITO anode as its higher work function lowers the energy barrier at the interface of ITO/organic donor layer [9]. Poly(3, 4-ethylenedioxythiophene) : poly(styrenesulfonate) (PEDOT : PSS) is one of the most commonly used hole-extracting layers in OSCs. However, PEDOT : PSS is burdened with electrical inhomogeneity which limits electron blocking capability as well as acidic nature which limits the stability and the lifetime of the device [10, 11]. This has driven the vigorous development of better hole-extracting layers. Recent literatures have extensively focused on transition metal oxides (TMO) because of their favorable electronic properties, low optical absorption in the visible spectrum, and high level of technological compatibility in organic electronics [12]. For example, molybdenum trioxide (MoO_3) [13], vanadium pentoxide (V_2O_5) [14], and tungsten trioxide (WO_3) [15] have been shown to be promising alternatives to PEDOT : PSS.

In our previous study, we had investigated the rubrene/C_{70}-based OSCs, which provided an open-circuit voltage (V_{OC}) almost twice as high as that of devices based on CuPc/C_{60} [16, 17]. In this paper, we first demonstrate an improvement in rubrene/C_{70}-based OSCs efficiency by inserting a transparent metal oxide V_2O_5 thin film as the hole-extracting layer. The effects of the morphology and the thickness of the V_2O_5 interlayer on the performance of OSC were investigated. The efficiency is improved in OSC with optimized thickness of V_2O_5 interlayer, which is higher than that with bare ITO by about 3 times. The mechanism is discussed from perspectives of change in resistance, the film transparency, and the charge transport behavior. Our findings contribute to our understanding of hole-extracting

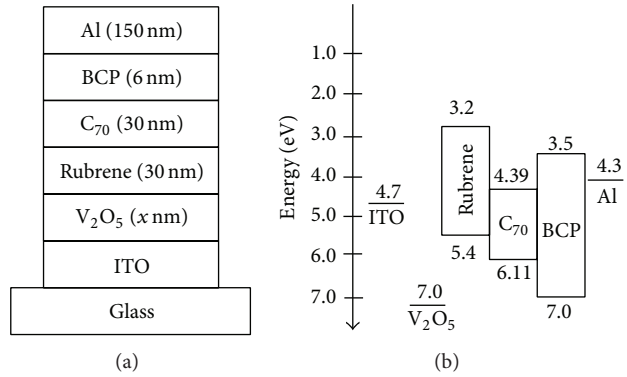

Figure 1: (a) Device structure of rubrene/C_{70}-based OSCs and (b) diagram of the energy level in OSCs.

behavior in OSCs and may be helpful in fabricating an efficient conversion contact layer in tandem OSCs [18, 19].

2. Materials and Methods

Cells were fabricated on commercially available ITO thin film coated glass substrates (180 nm ITO thickness with a sheet resistance less than 10 Ω/□). After successive ultrasonic cleaning processes in acetone, ethanol, and deionized water for 15 minutes each, the ITO glass was then dried by high-purity nitrogen flow before deposition. The organic and metal oxide layers were grown by vacuum deposition in a vacuum thermal evaporation system with a base pressure of 6×10^{-6} mbar. The organic materials used in cells were rubrene (99%), C_{70} (99%), and 2,9-dimethyl-4,7-diphenyl-1,10-phenanthroline (BCP) (99%) without further sublimation before deposition. The V_2O_5 (99%) was used as received. An aluminum thin film with the thickness of 150 nm was deposited *in situ* as the cathode electrode. The deposition rates of V_2O_5, rubrene, C_{70}, BCP, and Al were 0.05–0.1/s, 0.06–0.15 nm/s, 0.8–1.5 Å/s, 0.01–0.04 nm/s, and 1.0–4.0 nm/s, respectively. The thickness of layers was monitored by an INFICON XTM/2 oscillating quartz thickness monitor. The schematics of cell structure and energy level are shown in Figures 1(a) and 1(b).

The active area of the device irradiated was 0.5×0.6 mm^2. Current density-voltage (J-V) characteristics were measured with a Keithley 2400 sourcemeter under an illumination of 100 mW/cm^2 with an AM 1.5G solar illumination from ABET Technologies, Sun 2000 Solar simulator. The solar cell was calibrated using a reference Si solar cell. The surface morphology of V_2O_5 interlayer was analyzed by atomic force microscope (AFM, CSPM 5500), and the transmission spectra of the V_2O_5 interlayer were measured by UV-Vis spectrophotometer (UV-2550). All measurements were carried out in ambient air without any encapsulation.

3. Results and Discussion

Cells with the architecture ITO/V_2O_5 (0 or 3 nm)/rubrene (30 nm)/C_{70} (30 nm)/BCP (6 nm)/Al (150 nm) (Figure 1(a)) were fabricated. Figure 2 shows J-V characteristics of the device with 0 and 3 nm thick V_2O_5 layer under 100 mW/cm^2

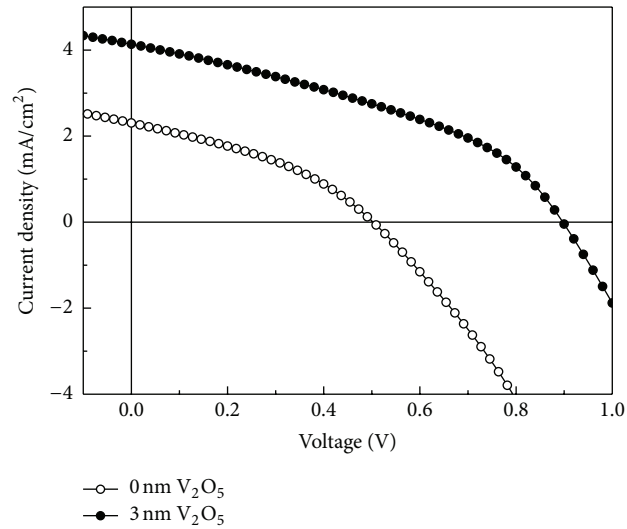

Figure 2: The J-V characteristics of devices under 100 mW/cm^2 white light illumination in air: ITO/V_2O_5 (3 nm)/Rubrene/C_{70}/BCP/Al (solid circle) and ITO/Rubrene/C_{70}/BCP/Al (open circle).

white light illumination. In the absence of V_2O_5 interlayer, the simple device presents a power conversion efficiency of 0.42% with a low fill factor of 36.2%. The J_{SC} and V_{OC} are 2.3 mA/cm^2 and 0.51 V, respectively. However, by inserting a 3 nm V_2O_5 interlayer between the donor layer and anode, the device exhibits a significant improvement in power conversion efficiency (PCE) to 1.74%, with short-circuit current density (J_{SC}) 4.58 mA/cm^2, open-circuit voltage (V_{OC}) 0.88 V, and fill factor (FF) 43.3%.

Figure 1(b) shows the diagram of energy level in the rubrene/C_{70}-based OSC [11, 20, 21]. Due to high work function, the thermally evaporated ultrathin film of V_2O_5 has a more favorable energy level alignment for hole extraction compared to bare ITO [22]. Figure 3 shows the surface morphology of ITO and ITO covered with a 3 nm V_2O_5 interlayer. The surface of ITO substrate shows a root-mean-square (RMS) roughness of 1.81 nm. After covering with a 3 nm thick V_2O_5 layer, the RMS roughness decreases to 1.46 nm. ITO

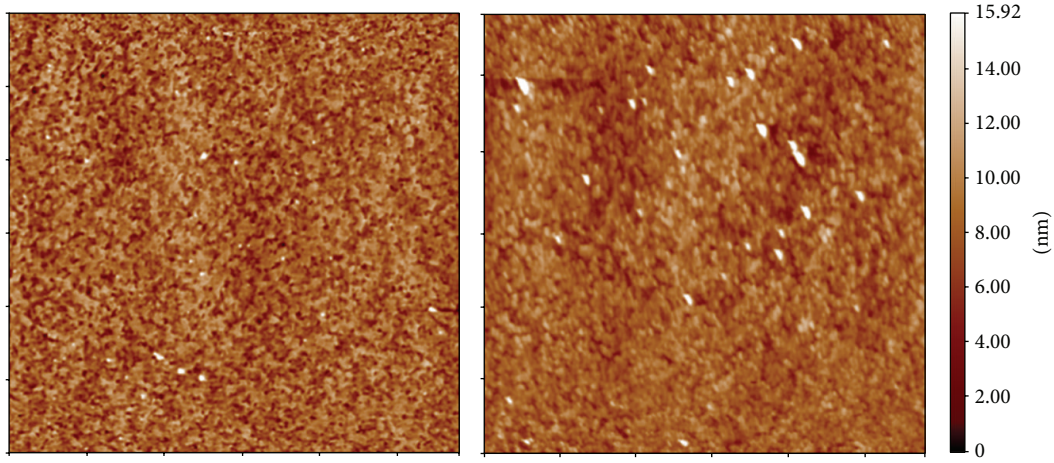

FIGURE 3: The surface morphology of (a) ITO and (b) ITO coated with 3 nm of V_2O_5 interlayer. The area is $29 \times 29\ \mu m^2$.

with improved morphology will favor the contact between the anode layer and the donor layer [23]. Some small islands were observed on the surface of ITO covered with 3 nm V_2O_5, which were made of oxide molecules aggregated together on the surface. Minimization of the surface energy might play a role in the formation of such islands which occupy a very small amount of surface area, and the V_2O_5 layer below the islands should dominate the performance [24].

By introducing a 3 nm V_2O_5 hole-extracting layer, the device shows a remarkable increase in J_{SC} from 2.30 mA/cm^2 to 4.58 mA/cm^2. It is known that the resistance of the active materials and the contact resistance contribute to the series resistance. Theoretically, inserting a V_2O_5 layer will introduce two additional interfaces (rubrene/V_2O_5 and V_2O_5/ITO) which contribute to an increase in the contact resistance, therefore, increasing the series resistance. However, the series resistance (R_S, defined by the slope of the J-V curve at $J = 0$ mA/cm^2) is estimated to be 40 and 95.7 Ω cm^2 for the device with and without V_2O_5 interlayer, respectively. Consequently, the decrease in series resistance of the device indicates that the insertion of V_2O_5 interlayer suppresses the contact resistance remarkably. Although most of the carriers are generated in the active layer, their collection is relative to the contact resistance at the organic/electrode interface [25]. Besides, the high work function of V_2O_5 (7.0 eV) [9] will enhance hole collection at the organic/ITO interface.

It is observable that the cell without a V_2O_5 hole-extracting layer exhibits a low V_{OC} of 0.51 V, which leads to a lower PCE. However, by incorporating a hole-extracting layer, the V_{OC} has an obvious increase to 0.88 V. Providing a more favorable energy level alignment with the donor HOMO than ITO does, and decreasing the series resistance, the hole-extracting layer allows for an Ohmic contact and decreases the losses in the built-in field, leading to the increase in the V_{OC} since the V_{OC} is the voltage where the applied bias equals the built-in potential in an ideal diode [22, 26]. Similar to J_{SC} and V_{OC}, the FF also has an increase from 36.2% to 43.3%. The decrease in series resistance and the better transport property contribute to the increase in FF.

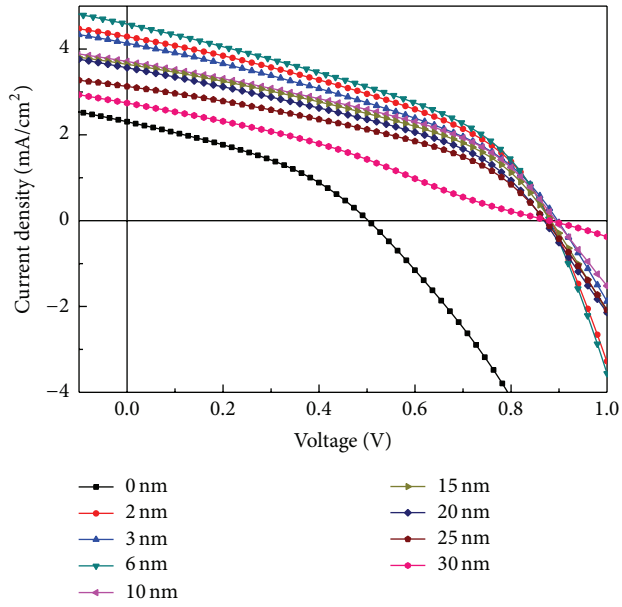

FIGURE 4: The J-V characteristics of devices with variable V_2O_5 interlayer under 100 mW/cm^2 white light illumination in air.

As a consequence, the performance of the device with metal oxide is better as compared to the ITO-only device.

For V_2O_5 placed between ITO and the donor layer, an overall increase in J_{SC}, V_{OC}, and FF is obtained, which offers a substantial improvement in PCE. However, introducing a thinner layer of V_2O_5 will generally lead to a low V_{OC} and a high leakage current, while a thicker layer will result in an increased series resistance, consequently reducing the J_{SC} and FF. To find out the optimum thickness, the effect of V_2O_5 interlayer thickness on device performance is investigated and showed in Figure 4. The detailed result is summarized in Table 1.

There is a pronounced dependency of device performance on the thickness of V_2O_5 interlayer and the optimum V_2O_5

Table 1: Characteristics (η_P, J_{SC}, V_{OC}, FF, and R_S) of OSCs with V_2O_5 as the hole-extracting layer (varied thickness). The optimum V_2O_5 thickness is 3 nm (bold values).

Hole-extracting layer (nm)	PCE (%)	J_{SC} (mA/cm^2)	V_{OC} (V)	FF (%)	R_S (Ω cm^2)
0	0.425	2.304 ± 0.2	0.51 ± 0.05	36.2 ± 0.6	95.7
2	1.557	4.289 ± 0.2	0.88 ± 0.01	41.2 ± 0.7	43.0
3	**1.745**	**4.583 ± 0.2**	**0.88 ± 0.01**	**43.3 ± 0.1**	**40.0**
6	1.651	4.606 ± 0.3	0.88 ± 0.01	40.8 ± 0.4	41.2
10	1.390	3.711 ± 0.1	0.90 ± 0.02	41.6 ± 0.8	68.0
15	1.320	3.642 ± 0.06	0.88 ± 0.01	41.2 ± 0.3	59.5
20	1.238	3.563 ± 0.1	0.86 ± 0.02	40.4 ± 1.0	63.2
25	1.110	3.128 ± 0.2	0.88 ± 0.02	40.3 ± 1.0	71.5
30	0.731	2.742 ± 0.1	0.88 ± 0.01	30.3 ± 1.0	365

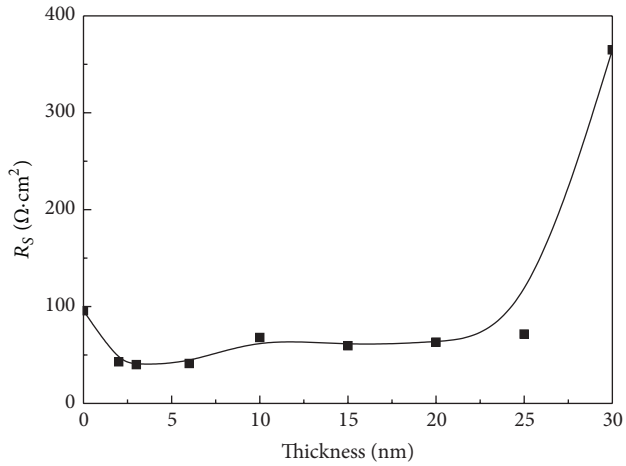

Figure 5: The curve of series resistance-thickness of V_2O_5 interlayer.

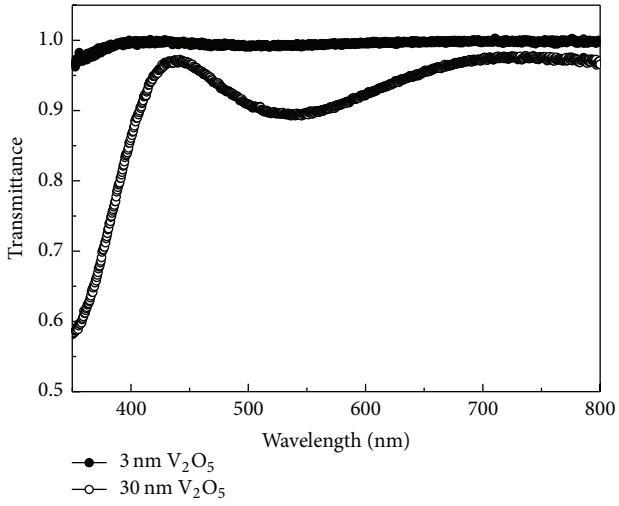

Figure 6: Transmission spectra of the V_2O_5 layer with a thickness of 3 nm (solid circle) and 30 nm (open circle) on ITO.

thickness for our device is 3 nm (bold values in Table 1). When the thickness is 2 nm, the ITO will not be fully covered by V_2O_5 and two interfaces (V_2O_5/ITO and organic/ITO) are formed. Therefore, the *J-V* curve of the cell with 2 nm thick V_2O_5 interlayer can be considered as the overlapping of two independent *J-V* curves of cells with 3 nm of V_2O_5 interlayer and without V_2O_5. Due to the bad performance of a cell without V_2O_5, the overlapping curve will result in a worse performance than that of a cell with 3 nm thick V_2O_5 layer, as is shown in Figure 4.

With the thickness of V_2O_5 increasing from 3 nm to 30 nm, the V_{OC} and FF changed slightly. On the contrary, the J_{SC} of a cell with 3 nm thick V_2O_5 layer is approximately higher than that of a cell with 30 nm V_2O_5 interlayer by one time. The deterioration of characteristics for devices with V_2O_5 interlayer thickness larger than 3 nm may be due to the reduction in the quality of both electrical conductivity and optical transmissivity of the V_2O_5 interlayer [11]. Firstly, we estimated the series resistance of cells with different thickness of V_2O_5 shown in Table 1. Figure 5 shows the R_S/R_{S0}-V_2O_5 interlayer thickness curve (R_{S0}, defined as the series resistance of a device with 0 nm thick V_2O_5 layer). As compared to that of the optimum cell, the series resistance of cells with thicker V_2O_5 film increases, which indicates that the electrical conductivity becomes worse with the increase of the V_2O_5 thickness from 3 nm to 30 nm. The series resistance of the cell with 30 nm V_2O_5 interlayer is almost 10 times higher than of that with 3 nm thick V_2O_5 layer.

We also investigated the optical properties of V_2O_5 films shown in Figure 6. With a thickness of 30 nm interlayer, the V_2O_5 film shows significant optical absorption in the visible band and wavelengths below 400 nm. Based on the transmittance data, we propose that a V_2O_5 layer with the thickness of 3 nm almost transmits 100% of light intensity at wavelength higher than 390 nm whilst a 30 nm V_2O_5 interlayer absorbs 23% of light intensity at 390 nm (the maximum of the spectral absorption of C_{70}). At 350 nm wavelength, a 3 nm thick layer transmits 96% of the photons while a 30 nm thick layer only transmits 58% of light intensity, which is similar to the result reported by Zilberberg et al. [11]. Thus, it appears reasonable that the deterioration of cell performance with thicker V_2O_5 (>3 nm) interlayer is related

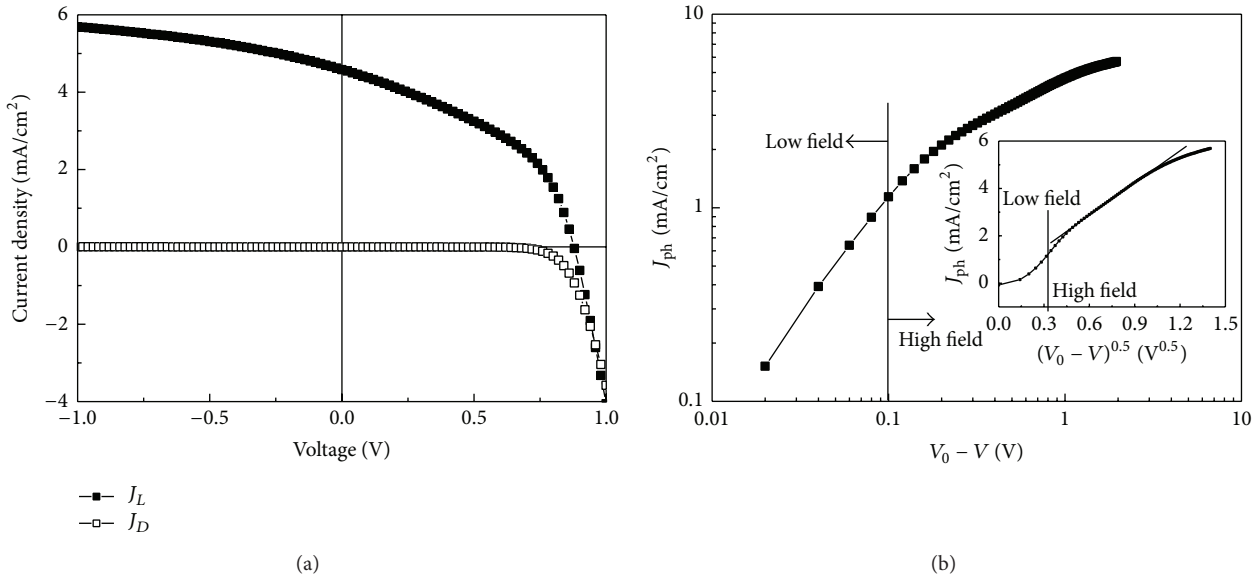

FIGURE 7: (a) The J-V characteristics of the device with a 3 nm thick V_2O_5 layer in the dark (open square) and under white light illumination of 100 mW/cm^2 (solid square). (b) The photocurrent J_{ph}-effective applied bias voltage ($V_0 - V$) curve of device with a 3 nm V_2O_5 interlayer.

to the lower electrical conductivity and optical transmissivity of the V_2O_5.

The typical FF of OSCs based on small molecules is typically between 0.5 and 0.65 [5]. But as-prepared rubrene/C_{70}-based OSCs have the highest FF of 43.3%, which is much lower than the typical value. The reverse bias photocurrent J_{ph} ($J_{ph} = J_L - J_D$, J_L, and J_D are defined as the current density of the device under illumination with 100 mW/cm^2 white light and in the dark) of a device with FF > 50% saturates at the high reverse bias, indicating the fact that almost all the photogenerated free charge carriers are extracted [27]. However, in Figure 7(a), the J_{ph} in the reserve bias shows strong field dependence. In other words, the exciton dissociation rate of a device with 3 nm interlayer is moderately dependent on voltage.

Besides the field-dependent exciton dissociation rate, unbalanced transports of charge carriers also play a role in reducing the FF. Figure 7(b) shows the J_{ph}-($V_0 - V$) curve of optimum device (V_0 is the compensation voltage, defined as the voltage at $J_{ph} = 0$, here V_0 is equal to 0.96 V). At low effective field ($V_0 - V \leq 0.1$), J_{ph} shows linear dependence on the voltage, due to the competition between drift and diffusion of photogenerated free charges to the electrodes [28]. However, at high effective field ($V_0 - V \geq 0.1$), J_{ph} clearly illustrates a square-root dependence on the voltage, especially, at the field range from 0.2 V to 1 V, which can be clearly seen from the inset of Figure 7(b). During this field region, in case of mobility-lifetime limit, the J_{ph} is given by

$$J_{ph} = qG\left[(\mu\tau)_{\text{slow carrier}}\right]^{0.5} V^{0.5}, \quad (1)$$

where q is the electric charge, G is the generation rate, μ is the charge carrier mobility, and τ is the charge carrier lifetime.

While in case of space charge limit, the J_{ph} can be described by

$$J_{ph} = q\left(\frac{q\varepsilon_0\varepsilon_r\mu_{\text{slow carrier}}}{8q}\right)^{0.25} G^{0.75}V^{0.5}. \quad (2)$$

where $\varepsilon_0\varepsilon_r$ is the dielectric permittivity. Therefore, the J_{ph} is influenced by the unbalanced transport in the case of space charge limit or mobility-lifetime limit. For a photocurrent varying with a square-root dependence on the applied voltage, the FF amounts to 42% [27, 28]. It appears from Figure 7(b) that J_{ph} does not saturate with effective voltages exceeding 1 V but gradually increases for larger effective voltage. That is mainly because not all the photogenerated bound e-h pairs dissociate into free charge at the field lower than 1 V and the dissociation of a fraction of bound e-h pairs is dependent on field [29]. Hence, to some extent, the lower FF in rubrene/C_{70}-based OSC is due to the field-dependent J_{ph} as well as unbalanced transport.

4. Conclusions

We have explored the role of V_2O_5 hole-extracting layer in rubrene/C_{70}-based OSCs. Due to the favorable electronic properties, V_2O_5 interlayer effectively extracts holes and suppresses the contact resistance. Because of the thickness-dependent electrical conductivity and the optical transmissivity of the V_2O_5 layers, the performance of OSCs changes differently with the thickness of V_2O_5 layer. The highest PCE of 1.745% is achieved for the device with a 3 nm thick V_2O_5 interlayer and a high V_{OC} of 0.88 V is also obtained. As V_2O_5 interlayer can be used as the conversion contact layer in the tandem device, this work may contribute to further development of tandem solar cells.

Conflict of Interests

The authors declare that there is no conflict of interests regarding the publication of this paper.

Acknowledgments

The authors thank Professor W. J. Mai for his helpful discussion and thank the Natural Science Foundation of Guangdong Province, China (S2011010002575 and S2013010012856), the Open Fund of the State Key Laboratory of Luminescent Materials and Devices (South China University of Technology), and the National Natural Science Foundation of China (61274062 and 11204106) for partially supporting this study.

References

[1] J. Y. Kim, K. Lee, N. E. Coates et al., "Efficient tandem polymer solar cells fabricated by all-solution processing," *Science*, vol. 317, no. 5835, pp. 222–225, 2007.

[2] F. C. Krebs, H. Spanggard, T. Kjær, M. Biancardo, and J. Alstrup, "Large area plastic solar cell modules," *Materials Science and Engineering B*, vol. 138, no. 2, pp. 106–111, 2007.

[3] L. Blankenburg, K. Schultheis, H. Schache, S. Sensfuss, and M. Schrödner, "Reel-to-reel wet coating as an efficient up-scaling technique for the production of bulk-heterojunction polymer solar cells," *Solar Energy Materials and Solar Cells*, vol. 93, no. 4, pp. 476–483, 2009.

[4] C. W. Tang, "Two-layer organic photovoltaic cell," *Applied Physics Letters*, vol. 48, no. 2, pp. 183–185, 1986.

[5] K. L. Mutolo, E. I. Mayo, B. P. Rand, S. R. Forrest, and M. E. Thompson, "Enhanced open-circuit voltage in subphthalocyanine/C_{60} organic photovoltaic cells," *Journal of the American Chemical Society*, vol. 128, no. 25, pp. 8108–8109, 2006.

[6] P. Sullivan, A. Duraud, N. Beaumont et al., "Halogenated boron subphthalocyanines as light harvesting electron acceptors in organic photovoltaics," *Advanced Energy Materials*, vol. 1, no. 3, pp. 352–355, 2011.

[7] Y. Zhou, M. Eck, and M. Krüger, "Bulk-heterojunction hybrid solar cells based on colloidal nanocrystals and conjugated polymers," *Energy and Environmental Science*, vol. 3, no. 12, pp. 1851–1864, 2010.

[8] S. Schumann, S. A. F. Bon, R. A. Hatton, and T. S. Jones, "Open-cellular organic semiconductor thin films by vertical co-deposition using sub-100 nm nanosphere templates," *Chemical Communications*, no. 42, pp. 6478–6480, 2009.

[9] J. Meyer, K. Zilberberg, T. Riedl, and A. Kahn, "Electronic structure of vanadium pentoxide: an efficient hole injector for organic electronic materials," *Journal of Applied Physics*, vol. 110, no. 3, Article ID 033710, 2011.

[10] H. Yan, P. Lee, N. R. Armstrong et al., "High-performance hole-transport layers for polymer light-emitting diodes. Implementation of organosiloxane cross-linking chemistry in polymeric electroluminescent devices," *Journal of the American Chemical Society*, vol. 127, no. 9, pp. 3172–3183, 2005.

[11] K. Zilberberg, S. Trost, H. Schmidt, and T. Riedl, "Solution processed vanadium pentoxide as charge extraction layer for organic solar cells," *Advanced Energy Materials*, vol. 1, no. 3, pp. 377–381, 2011.

[12] J. Meyer, S. Hamwi, M. Kröger, W. Kowalsky, T. Riedl, and A. Kahn, "Transition metal oxides for organic electronics: energetics, device physics and applications," *Advanced Materials*, vol. 24, no. 40, pp. 5408–5427, 2012.

[13] M. Kröger, S. Hamwi, J. Meyer, T. Riedl, W. Kowalsky, and A. Kahn, "P-type doping of organic wide band gap materials by transition metal oxides: a case-study on molybdenum trioxide," *Organic Electronics: Physics, Materials, Applications*, vol. 10, no. 5, pp. 932–938, 2009.

[14] J.-S. Huang, C.-Y. Chou, M.-Y. Liu, K.-H. Tsai, W.-H. Lin, and C.-F. Lin, "Solution-processed vanadium oxide as an anode interlayer for inverted polymer solar cells hybridized with ZnO nanorods," *Organic Electronics: Physics, Materials, Applications*, vol. 10, no. 6, pp. 1060–1065, 2009.

[15] C. Tao, S. Ruan, G. Xie et al., "Role of tungsten oxide in inverted polymer solar cells," *Applied Physics Letters*, vol. 94, no. 4, Article ID 043311, 2009.

[16] Z. Chen, P. Liu, L. Hou, W. Mai, and B. Wu, "Optimization and degradation of rubrene/C_{70} heterojunction solar cells," *Optoelectronics Letters*, vol. 8, no. 2, pp. 93–96, 2012.

[17] J. Cao, Z. Zhan, L. Hou, Y. Long, P. Liu, and W. Mai, "Optical modeling of organic solar cells based on rubrene and C_{70}," *Applied Optics*, vol. 51, no. 23, pp. 5718–5723, 2012.

[18] J. Sakai, K. Kawano, T. Yamanari et al., "Efficient organic photovoltaic tandem cells with novel transparent conductive oxide interlayer and poly (3-hexylthiophene): fullerene active layers," *Solar Energy Materials and Solar Cells*, vol. 94, no. 2, pp. 376–380, 2010.

[19] W. Nie, R. C. Coffin, and D. L. Carroll, "Silver nanoparticle-doped titanium oxide thin films for intermediate layers in organic tandem solar cell," *International Journal of Photoenergy*, vol. 2013, Article ID 829463, 6 pages, 2013.

[20] D. Changgeng, Y. Jinlong, H. Rongsheng, and W. Kelin, "Formation mechanism and structural and electronic properties of metal-substituted fullerenes $C_{69}M$ (M = Co, Rh, and Ir)," *Physical Review A*, vol. 64, no. 4, Article ID 043201, 6 pages, 2001.

[21] D. Wang, Z. Wu, X. Zhang, D. Wang, and X. Hou, "Solution-processed white organic light-emitting devices based on small-molecule materials," *Journal of Luminescence*, vol. 130, no. 2, pp. 321–325, 2010.

[22] I. Hancox, L. A. Rochford, D. Clare, P. Sullivan, and T. S. Jones, "Utilizing n-type vanadium oxide films as hole-extracting layers for small molecule organic photovoltaics," *Applied Physics Letters*, vol. 99, no. 1, Article ID 013304, 2011.

[23] C.-J. Huang, J.-C. Ke, W.-R. Chen, T.-H. Meen, and C.-F. Yang, "Improved the efficiency of small molecule organic solar cell by double anode buffer layers," *Solar Energy Materials and Solar Cells*, vol. 95, no. 12, pp. 3460–3464, 2011.

[24] V. Shrotriya, G. Li, Y. Yao, C. Chu, and Y. Yang, "Transition metal oxides as the buffer layer for polymer photovoltaic cells," *Applied Physics Letters*, vol. 88, no. 7, Article ID 073508, 2006.

[25] C.-H. Lin, S.-C. Tseng, Y.-K. Liu et al., "Suppressing series resistance in organic solar cells by oxygen plasma treatment," *Applied Physics Letters*, vol. 92, no. 23, Article ID 233302, 3 pages, 2008.

[26] I. Hancox, P. Sullivan, K. V. Chauhan et al., "The effect of a MoO_x hole-extracting layer on the performance of organic photovoltaic cells based on small molecule planar heterojunctions," *Organic Electronics: Physics, Materials, Applications*, vol. 11, no. 12, pp. 2019–2025, 2010.

[27] D. Gupta, S. Mukhopadhyay, and K. S. Narayan, "Fill factor in organic solar cells," *Solar Energy Materials and Solar Cells*, vol. 94, no. 8, pp. 1309–1313, 2010.

[28] V. D. Mihailetchi, J. Wildeman, and P. W. M. Blom, "Space-charge limited photocurrent," *Physical Review Letters*, vol. 94, no. 12, Article ID 126602, 4 pages, 2005.

[29] V. D. Mihailetchi, L. J. A. Koster, J. C. Hummelen, and P. W. M. Blom, "Photocurrent generation in polymer-fullerene bulk heterojunctions," *Physical Review Letters*, vol. 93, no. 21, Article ID 216601, 4 pages, 2004.

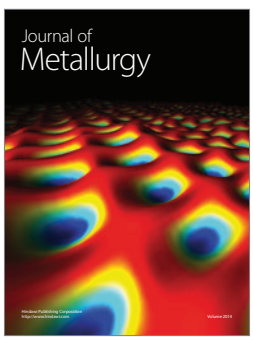

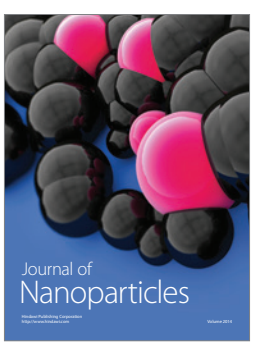

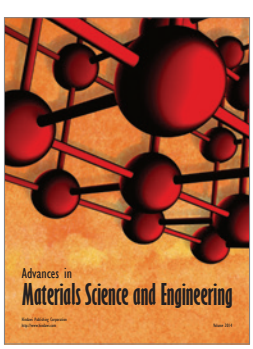

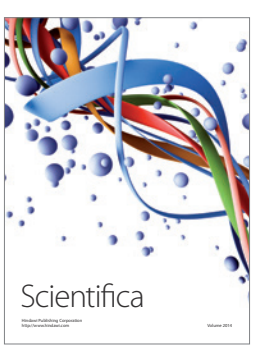

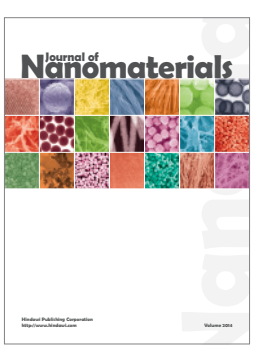

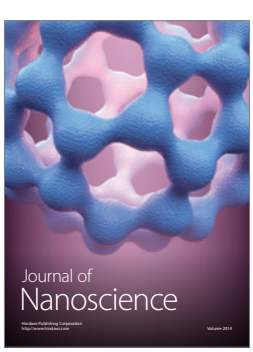

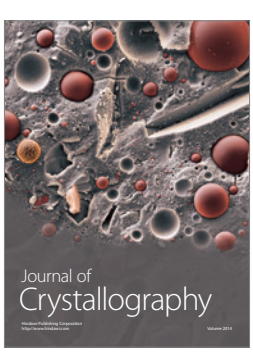

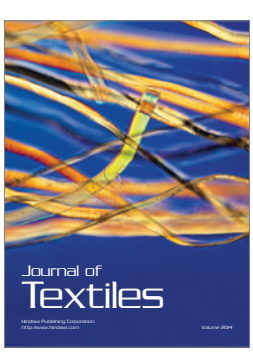

Hindawi

Submit your manuscripts at
http://www.hindawi.com